Optical mode localization sensing based on fibre-coupled ring resonators

SHUMENG WANG,[1] HAILONG PI,[1] YU FENG, [1] AND JIZE YAN[1,*]

[1] *School of Electronics and Computer Science, University of Southampton, Southampton SO17 1BJ, UK*
[*] *J.Yan@soton.ac.uk*

Abstract: Mode localization is widely used in coupled micro-electro-mechanical system (MEMS) resonators for ultra-sensitive sensing. Here, for the first time, we experimentally demonstrate the phenomenon of optical mode localization in fibre-coupled ring resonators. For an optical system, resonant mode splitting happens when multiple resonators are coupled. Localized external perturbation applied to the system will cause uneven energy distributions of the split modes to the coupled rings, this phenomenon is called the optical mode localization. In this paper, two fibre-ring resonators are coupled. The perturbation is generated by two thermoelectric heaters. We define the normalized amplitude difference between the two split modes as: $(T_{M1} - T_{M2})/T_{M1} \times 100\%$. It is found that this value can be varied from 2.5% to 22.5% when the temperature are changed by the value from 0K to 8.5K. This brings a ~ 2.4%/K variation rate, which is three orders of magnitude greater than the variation rate of the frequency over temperature changes of the resonator due to thermal perturbation. The measured data reach good agreement with theoretical results, which demonstrates the feasibility of optical mode localization as a new sensing mechanism for ultra-sensitive fibre temperature sensing.

1. Introduction

The phenomenon of the mode localization is widely studied in coupled micro-electro-mechanical system (MEMS) resonators [1]. When two identical resonators are weakly coupled, the perturbation of a small stiffness or mass in one resonator will result in the uneven distribution of the vibration energy over the whole system [2, 3]. The unevenly-distributed energy is reflected by the resonant amplitude ratio between resonant modes, which is strongly dependent on the magnitude of the perturbation. Compared with measuring the resonant frequency shifts in resonators, measuring the amplitudes variations of eigenstates caused by vibration localization in weakly coupled resonators provides two unique advantages for sensing applications. Firstly, The parametric sensitivity in terms of variation rate is enhanced by at least three orders of magnitudes [2–7]. Secondly, the intrinsic common mode rejection due to the differential measurement techniques significantly reduces the impact of the environmental perturbations, which leads to better temperature stability [7, 8].

Compared with MEMS resonators, optical resonators exhibit several advantages. Optical ring or disk resonators can achieve high quality factors without using vibration structures and vacuum conditions [9–11]. These devices show great diversity in scale, with a variety of sizes from micrometers (waveguide) [12] to meters (fibres) [9], which play a key role in integrated photonic circuits [13–15], sensing [16] and optical communication [17].

For optical resonators, resonant modes will be split when two resonators are weakly coupled [18]. By a localized perturbation, the induced changes in the refractive index and coupling coefficient will change the energy distribution to all resonant modes. These changes thereby result in asymmetrical splitting of the resonant modes. The symmetry feature of the mode splitting can be evaluated by the modal power ratio between two split modes, which can indicate the magnitude of the perturbation. Therefore the localized perturbation can be quantitatively measured by examining the modal power ratio between the split modes [3–6].

This sensing mechanism can be embedded in optical waveguide/fibre systems to develop ultra-sensitive sensors. In this paper, we experimentally investigate, for the first time, the optical mode localization in fibre-coupled ring resonators. In the experiment, two different coupled ring resonators (Device A with the coupling ratio $\kappa = 0.1$ and Device B with $\kappa = 0.5$. κ refers to the strength of the coupling between the resonator and the input/output fibres.) are fabricated. By tuning the thermal perturbation, the variations of the amplitude difference between the split modes are measured. For Device A, the difference can be tuned from -6% to -2% as the temperature variation increases from 0K to 8.5K, the corresponding variation rates are ~ -0.41%/K and ~ 0.39%/K when the upper and bottom rings are heated, respectively. In contrast, For Device B, the difference can be tuned from 2.5% to 22.5% when the temperature variation increases from 0K to 8.5K, the corresponding variation rates are ~ -2.2%/K and ~ 2.4%/K when the upper and bottom rings are heated, respectively. The demonstrated results exhibit three orders of magnitude improvement in the sensitivity in terms of variation rate to the temperature changes comparing with the variation rate of the thermally-induced frequency shift. Combining the advantages of optical fibres, we provide a new way for ultra-sensitive fibre temperature sensing.

2. Experiment setup

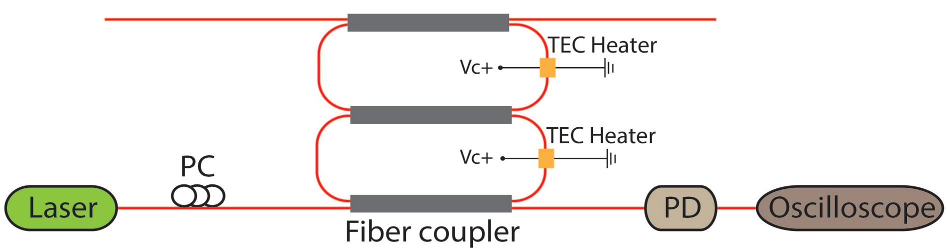

Fig. 1. Schematic of the system. The device consists of two coupled ring resonators, which are formed by three fibre couplers. Two thermoelectric (TEC) heaters are placed on the upper and bottom rings, respectively. The uneven distribution of optical energy will occur when only one of the heaters is utilized.

Figure. 1 is the schematic of the system. The coupled ring resonators are produced by fusion-splicing the output ports of 2×2 single-mode fibre couplers to their input ports. The circumference of each ring resonator is around 50 cm. A tunable laser with the linewidth of 1 MHz is used to measure the resonance response of the coupled ring resonator. A polarization controller is placed after the laser to ensure only one eigenmode is excited to the device [9]. The light signal from the output of the coupled ring resonator is captured and measured by a photodetector and an oscilloscope. In this experiment, the critical coupling is desired to ensure a high extinction ratio (ER). However, due to the unavoidable losses induced by the fibres, couplers and fusion splices, it is hard to achieve critical coupling by using fibre couplers with fixed coupling coefficients. Here, two coupling coefficients (0.1 and 0.5) are used to form two devices (Device A and B), and their performances are compared in this paper.

3. Transmission spectrum for the devices with different coupling coefficients

The spectrum of the devices without thermal perturbation is shown in figure. 2. The split notches M1 and M2 in the spectrum indicate two split resonant modes, which are called symmetric and antisymmetric modes [18, 19]. For one mode, the ER is defined as the difference between the on-resonance and off-resonance transmissions [12, 20]. To maximise ER, the coupling coefficient

κ and attenuation coefficient α have to be equal to reach the critical coupling. Figure. 2 (a) displays the transmission spectrum of Device A. In this situation, the maximum ER is 0.15, which indicates a massive gap between the κ and the α. Device B is also examined, which is shown in figure. 2 (b). It shows that when the κ is increased, the maximum ER increases from 0.15 to 0.4, which enlarges the initial ER by 160%. It is also found that the enlarged ER significantly improves the device's sensitivity to the temperature changes, which will be discussed later. It should be noticed that the initial ERs of the split modes shown in figure. 2 are different. This is because the two fabricated fibre-coupled ring resonators are not identical due to fabrication imperfection. Nevertheless, this will not affect the measurement because each time before the temperature is measured, the response without temperature perturbation is measured first and it will be used as an initial benchmark. When temperature perturbation is induced, the actual temperature change will be measured by the difference between the response and the pre-set benchmark.

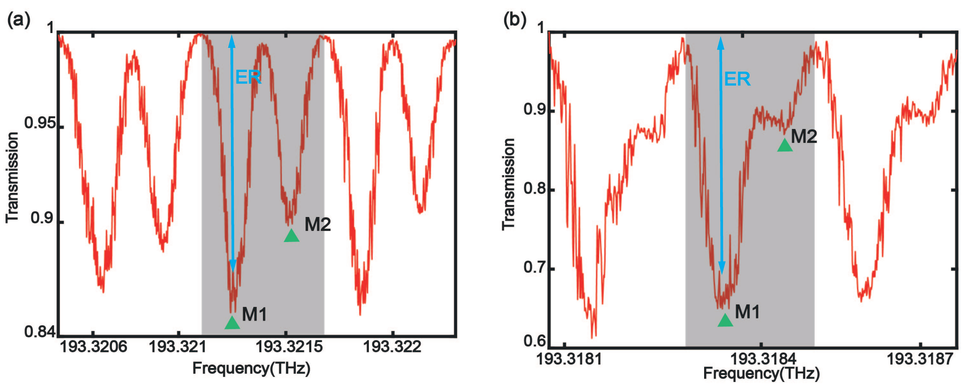

Fig. 2. Measured spectrum of the devices with different coupling coefficients: (a) Device A with $\kappa = 0.1$ and (b) Device B with $\kappa = 0.5$. The split notches M1 and M2 are the two split resonant modes. The gray area represents one period.

4. Simulation results

4.1. Fitting of the measured data

Figure. 3 (a) and (b) display the theoretical fits to the measured spectrum. The fitting functions are calculated by using the transfer matrix method [21], and also verified by the Lumerical interconnect module simulation. Before doing further analysis, a smoothing function is utilized to remove the glitches of the signal. Compare with the raw data shown in figure. 2, most glitches are removed after smoothing by a Gaussian window and the processed signals show good fits with the theoretical models.

4.2. The ERs of the split modes when the devce is heated

In this experiment, the thermal perturbation is induced by two thermoelectric (TEC) heaters, placed on the upper and bottom rings, respectively. The heating length that the TEC heaters can cover is 1 cm. Due to the thermal-optical effect, the refractive index of the covered coupled ring resonators will change according to the induced temperature variation. The thermal-optic coefficient is $1.33 \times 10^{-5} K^{-1}$ for silica optical fibre; therefore there will be 0.0000133 refractive index changes per K. We simulate the transmission responses with temperature variations, and the results are shown in figure. 3 (c) and (d). It can be seen that the variations of the two split

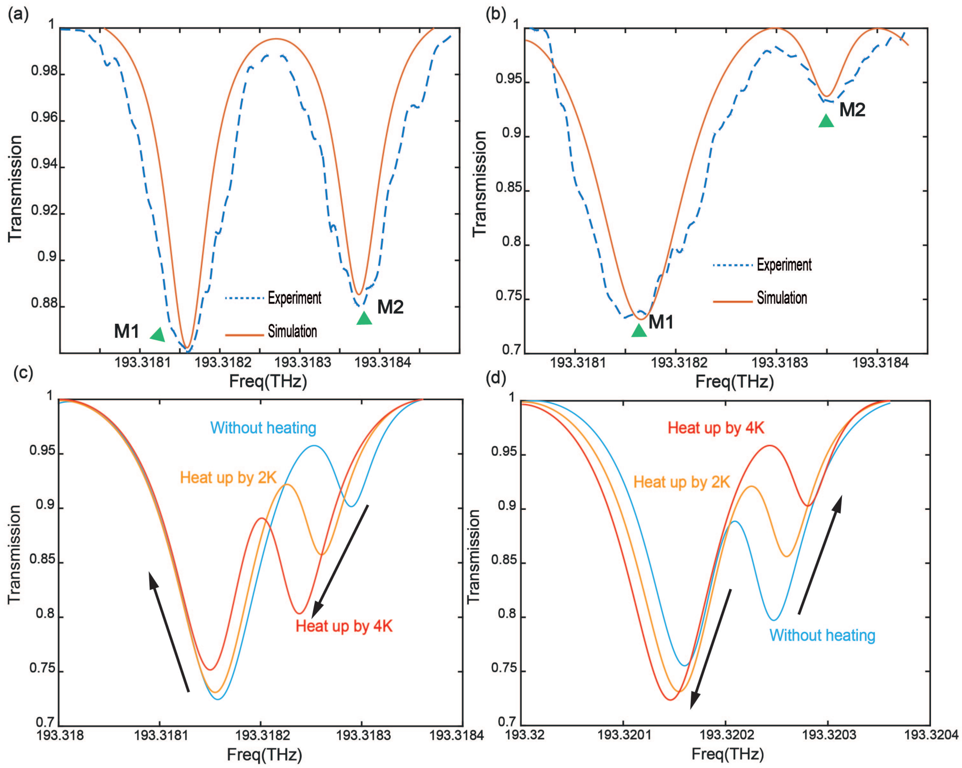

Fig. 3. (a) The theoretical fits to the measured spectrum for Device A. (b) The theoretical fits to the measured spectrum for Device B. (c) and (d) The changes of two split modes when temperature perturbation is induced, the simulation is based on $\kappa = 0.5$. (c) when the upper ring is heated. (d) when the bottom ring is heated.

modes show opposite trends when different rings are heated up, respectively. In figure. 3 (c), only the upper ring is heated. When the temperature is increased by the value from 0K (Blue line) to 4k (Red line), the ERs of M2 increase from 0.1 to 0.22 while the ERs of M1 drop from 0.28 to 0.25. Comparing with only heating the upper ring, the variations of M1 and M2 will be different if only the bottom ring is heated, which is shown in figure. 3 (d). The ERs of M2 reduce from 0.22 to 0.1 and the ERs of M1 increase from 0.24 to 0.28 as the bottom ring is heated. These opposite changes are due to the optical mode localization effect, it induces unevenly distributed energy to the split modes, which will be discussed in the next section.

4.3. The energy distributions of the split modes when the device is heated

After comparing the transmissions between different heating positions, it is found that heating the upper ring will cause opposite changes on the ERs of the two split modes regarding to heating the lower ring. This is due to the induced uneven optical energy distributions of the split modes to the two rings when different rings are heated. Based on our previous work, when the temperature of the upper ring increases, as shown in figure. 4 (a), the ER of M1 drops while the ER of M2 rises. This indicates that the energy of the mode M1 is more localized into the bottom ring. In contrast, for the mode M2, the optical energy is more localized into the upper ring. While heating the bottom ring will give opposite distributions, as shown in figure. 4 (b), the ER of M1 raises and the ER of M2 declines. In this case, the energy is more allocated into the upper ring when the mode M1 is pumped, and into the bottom ring when the mode M2 is pumped. In

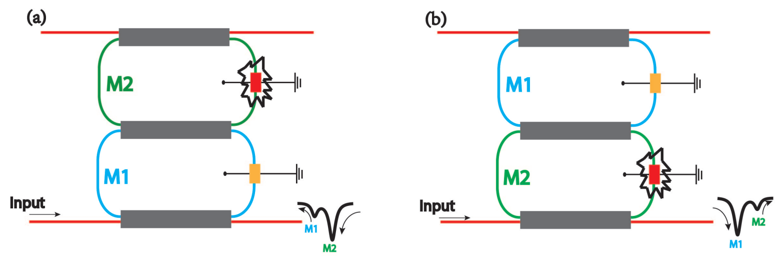

Fig. 4. The optical energy distributions of M1 and M2 when two rings are heated, respectively. (a) When the upper ring is heated. (b) When the bottom ring is heated.

conclusion, the energy distributions of the resonant modes are significantly influenced by the location of the heating source. Also, the energy concentration of M2 and M1 are proportional and inversely proportional to the temperature, respectively. In this way, we correlate the energy localization of the split modes to the measured ER changes, enabling us to utilize the measured thermally-induced ERs changes to quantify the energy distribution of the resonance modes.

4.4. The comparison between M1 and M2 when the temperature is changing

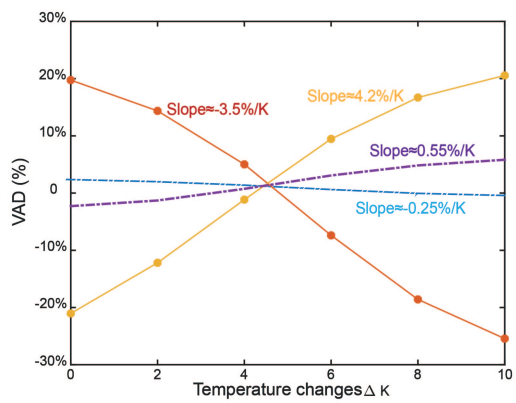

Fig. 5. The simulated results for the variation of VAD when the temperature is changing. Yellow line: the upper ring is heated, $\kappa = 0.5$. Red line: the bottom ring is heated, $\kappa = 0.5$. Purple line: the upper ring is heated, $\kappa = 0.1$. blue line: the bottom ring is heated, $\kappa = 0.1$.

In this experiment, the variation of the normalized amplitude difference (VAD) between M1 and M2 is used to quantify the induced thermal perturbation. VAD is defined as $VAD = ((T_{M1} - T_{M2})/T_{M1}) \times 100\%$, where T_{M1} and T_{M2} are the normalized amplitudes of the mode M1 and M2, respectively. When the upper ring or the bottom ring is heated, the VAD will vary with temperature. In figure. 5, Device A and Device B are evaluated, respectively. When Device A is tested, the significant difference between the attenuation coefficient α and coupling coefficient κ decreases ER, which limits the total range of amplitude changes. When the upper ring is heated (Blue line), the VAD is gradually decreasing from 2% to -1% as the temperature increases from 0k to 10k, the corresponding variation rate is $\sim -0.25\%$/K. In contrast, the VAD exhibits opposite trend when the bottom ring is heated (Purple line), which is gradually increasing from -2% to 5%, the corresponding variation rate is $\sim 0.55\%$/K. However, when the κ increases, enabling the coupled rings to approach critical coupling, the maximum ERs of both modes will increase. As shown by the yellow and red lines in figure. 5, the VAD is gradually changing between -25% to 20% as the temperature is increasing. The variation rates are $\sim -3.5\%/\text{K}$ and $\sim 4.2\%/\text{K}$ for the upper and bottom heating positions, respectively. The results show that under the same temperature changing range ΔK, the variation rate of VAD for Device B is four times higher than the Device A. In conclusion, the VAD variation rate is significantly relied on the maximum ER that the system can reach. Heating different positions gives opposite VAD variations, the variation is 0 when the transmissions of M1 and M2 are equal, which agrees with the theory.

4.5. Comparing with thermally-induced frequency-shift

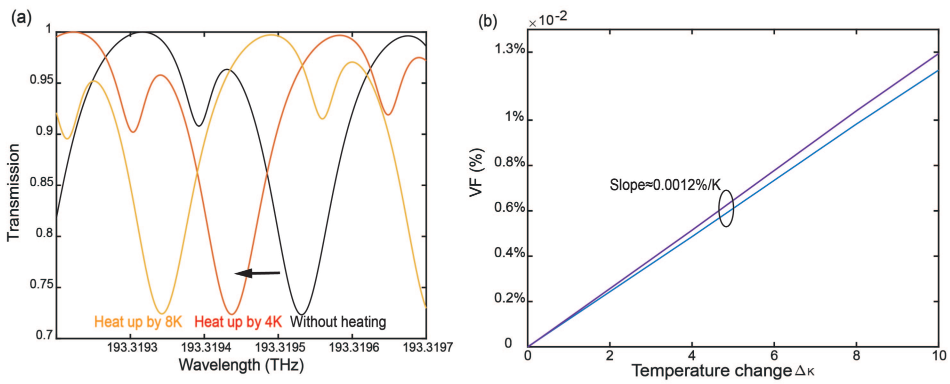

Fig. 6. (a) The simulated frequency shift when two rings are heated at the same time. (b) The variation of the VF when ΔT increases from 0K to 10K, purple line: M1, blue line: M2.

As the coupled ring resonator is heated, the frequency of the resonant mode will shift due to the thermal-optical effect. However, this shift is small as the thermal-optical coefficient is small. In theory, the resonant frequency shift that is due to the thermal-optical effect can be expressed as [22]:

$$f_r - f_0 = \frac{N}{n_g} \cdot f_r \cdot \Delta T \tag{1}$$

where f_0 and f_r are the resonant frequencies before and after thermal perturbation, respectively. N is the thermal-optical coefficient and n_g is the group index. Figure. 6 (a) displays the resonant frequency shift when both rings are heated. Both split modes are blue-shifted when the temperature increases. The resonant frequencies of modes M1 and M2 are shifted by 72MHz and 90MHz, respectively when the temperature is increasing by 8K. To evaluate the temperature sensitivity of the thermally-induced-frequency-shift-based sensing, we define the variation of the resonant frequency as $VF = ((f_r - f_0)/f_0) \times 100\%$, where f_0 and f_r are the resonant frequencies before and after the temperature changes. As shown in figure. 6 (b), when the temperature is increased by the value from 0K to 10K, both resonant frequencies shift at a similar rate. The variation rate of the VF is around 0.0012%/K. Comparing the VAD and the VF, it is found that the variation rate of the optical-mode-localization-effect-based VAD is about 3 orders of magnitude greater than the variation rate of the frequency-shift-based VF, and this can be further enhanced if the critical coupling is reached. Traditionally, fibre ring resonators are rarely used as temperature sensor because thermal optical effects are immaterial when using large cavities [22], only on-chip micro-resonators are eligible for temperature sensing [23, 24]. With the mode localization enhancement, the sensitivity to temperature changes improves by 3 orders of magnitude, which makes fibre-coupled ring resonators a potential ultra-high sensitive temperature sensor.

5. Experimental results

5.1. The temperature response of TEC heater

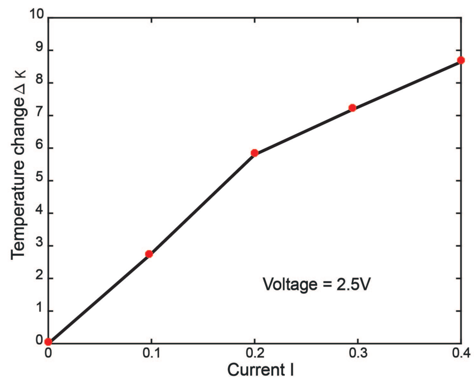

Fig. 7. The temperature response of TEC heater

Firstly, two TEC heaters are tested. The load voltage is fixed to 2.5V, as we gradually increase the current, the temperature responses are shown in figure. 7. The temperatures at I=0A, 0.1A, 0.2A and 0.4A will be used to test our devices.

5.2. Transmission responses when the devices are heated

Figure. 8 displays the measured transmission responses when the upper or bottom ring is heated. In the experiment, both devices are heated up by the value from 0K to 8.5K. For Device A, The ER of M1 decreases from 0.16 to 0.13 when the upper ring is heated and increases from 0.09 to 0.12 when the bottom ring is heated, respectively. In contrast, the ER of M2 increases from 0.09 to 0.12 when the upper ring is heated and decreases from 0.16 to 0.13 when the bottom ring is heated, respectively. The results are shown in figure. 8 (a) and (b). When Device B is tested, the coupling coefficient κ increases from 0.1 to 0.5. As shown in figure. 8 (c) and (d), the variations of M1 and M2 show the same trends as Device A, but as the temperature increases, the steps of the variations become larger. the ER of M1 decreases from 0.12 to 0.04 when the upper ring is heated and increases from 0.06 to 0.15 when the bottom ring is heated, respectively. In contrast, the ER of M2 increases from 0.17 to 0.23 when the upper ring is heated and decreases from 0.27 to 0.16 when the bottom ring is heated, respectively. Overall, increasing the coupling coefficient κ from 0.1 to 0.5 enables the coupled rings to approach critical coupling, which improves the maximum ERs of both modes. The measured opposite ERs changes of two modes with temperature also show good agreement with the theoretical results shown in figure. 3 (c) and (d).

5.3. The variation of VAD during temperature changes

To evaluate the device's sensitivity to the temperature changes, the variation of VAD is calculated based on the recorded transmissions. Figure. 9 (a) displays the VAD variation at 0K, 2.5K, 5.8K and 8.5K heated temperature. For Device B, the variation of the VAD ranges from 2.5% to 22.5%. The corresponding variation rate is $\sim -2.2\%/K$ when the upper ring is heated and $\sim 2.6\%/K$ when the bottom ring is heated. In contrast, for Device A, the variation range of VAD is limited

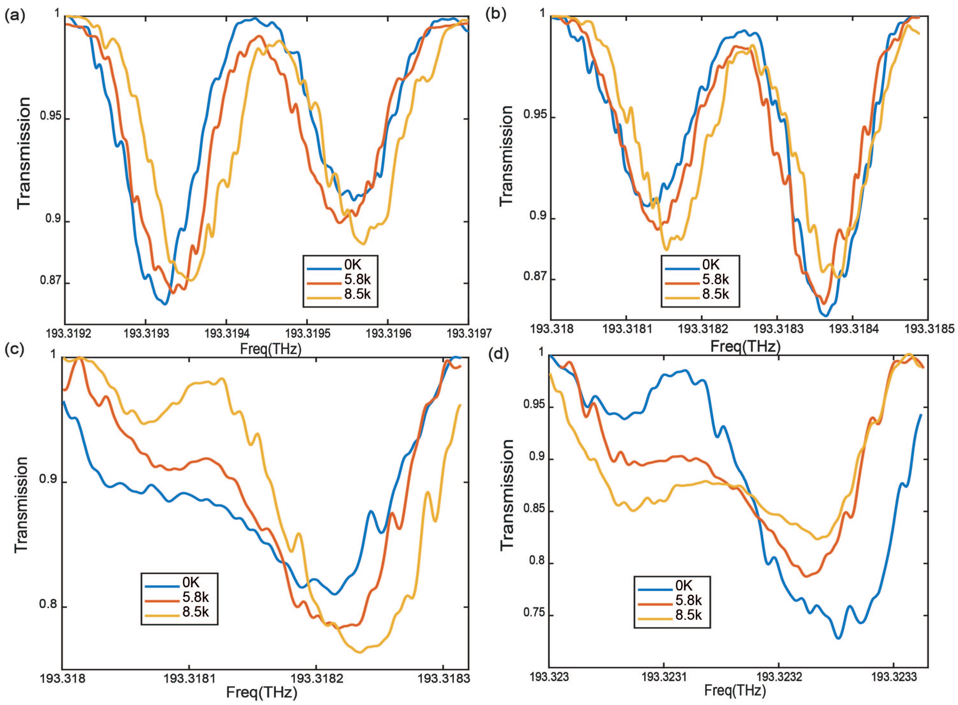

Fig. 8. The transmission response of the device with (a) $\kappa = 0.1$ when the upper ring is heated, (b) $\kappa = 0.1$ when the bottom ring is heated, (c) $\kappa = 0.5$ when the upper ring is heated (d)$\kappa = 0.5$ when the bottom ring is heated. The inset is the temperature changes induced by TEC heaters.

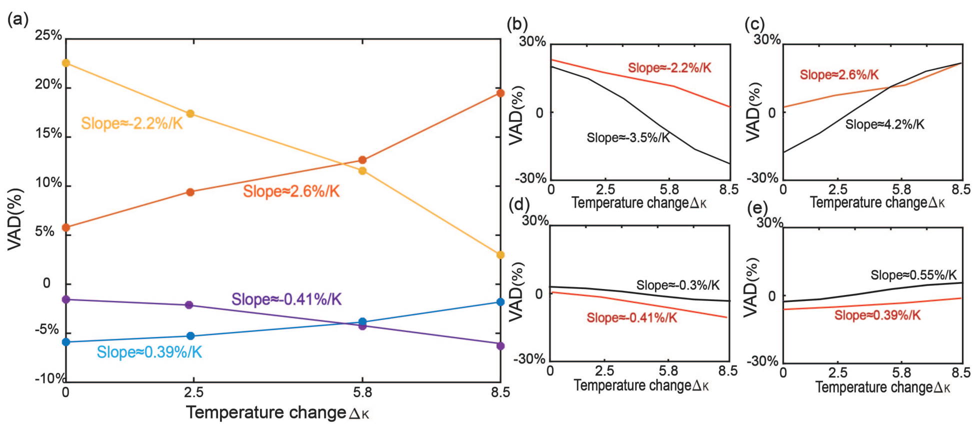

Fig. 9. (a) The results for the variation of VAD with temperature changes. Yellow line: $\kappa = 0.5$, the upper ring is heated. Orange line: $\kappa = 0.5$, the bottom ring is heated. Purple line: $\kappa = 0.1$, the upper ring is heated. Blue line: $\kappa = 0.1$, the bottom ring is heated. (b)-(e) The comparisons between the simulated (Black line) and the measured (Red line) VADs: (b) $\kappa = 0.5$, the upper ring is heated. (c) $\kappa = 0.5$, the bottom ring is heated. (d) $\kappa = 0.1$, the upper ring is heated. (e) $\kappa = 0.1$, the bottom ring is heated.

within -6% to -2%. The variation rates are $\sim -0.41\%/K$ and $\sim 0.39\%/K$ for the upper and bottom heating positions, respectively, which is around six times lower than Device A. The result is similar to our simulated one shown in figure. 5, where the variation rate of VAD improves by four times when increasing κ from 0.1 to 0.5. Figure. 5 (b)-(e) show the comparisons of VADs between the simulations and the measured results. It is found that the variation rates of the VADs of the measured results are slightly lower than the simulation results except when $\kappa = 0.1$ and the upper ring is heated, where the variation rate is $\sim -0.41\%/K$ in the experiment and $\sim -0.3\%$ in the simulation. In addition, the maximum error occurs when $\kappa = 0.5$ and the upper ring is heated, which is shown in figure. 5 (c), the variation rate in the experiment is $\sim 1.6\%$ lower than the simulation. Nevertheless, the experiment results exhibit at least three orders of magnitude higher variation rate if compared with the thermally-induced-frequency-shift-based sensing.

6. Discussion

Through theoretical and experimental studies, the phenomenon of optical mode localization due to the temperature perturbation in fibre-coupled ring resonators has been demonstrated. The device's sensitivity to temperature changes is improved by at least 3 orders of magnitude compared with frequency-shift-based sensing. In the experiment, the couplings of the fibre couplers are fixed so that it's hard to balance between the loss-induced attenuation factor α and coupling coefficient κ. Therefore the critical coupling is hard to reach to maximize ER. If replacing them by tunable couplers, the sensitivity could be even higher.

In this experiment, the data for each measurement is obtained by averaging three replicate measurements. This approach effectively reduces the experimental errors caused by optical noise originated from the detector, laser power, external vibration, etc [25]. Due to the limited size of the fibre ring resonator, where a minimum circumference of 30cm has been reported [9], the FSR is within the range of hundreds megahertz. In this case, laser with good frequency resolution (narrow linewidth) is required. In this experiment, the measured minimum FSR of our device is 400 MHz, which is shown in figure. 3. The linewidth of the laser is 1MHz, which means 400 points can be measured for each period. In addition, random de-tuning will also happen because the laser has reached its maximum tunable linewidth. Therefore, laser with narrower linewidth can be used to improve the accuracy of the measurement.

The system can be potentially used for ultra-sensitive temperature fibre sensing. In addition, comparing with on-chip integrated photonic sensors, fibre-coupled ring resonators offer larger scale for sensing range. Also, due to the flexibility of optical fibres, the sensing objects can be more than just regular shapes, which enables sensing under various conditions.

7. Conclusion

In summary, we experimentally demonstrate the optical mode localization in fibre-coupled ring resonators and its feasibility for high-sensitive sensing. Two fibre-coupled ring resonators with different coupling coefficients (Device A and Device B) are fabricated by fusion-spliced fibre couplers, the thermal perturbations are induced by two TEC heaters covered on the upper and the bottom ring resonators, respectively. The VAD variation rate of $\sim 2.3\%/K$ is achieved when the coupling coefficient is 0.5, which is three orders of magnitude greater than the variation rate of the frequency-shift-based VF. The value can be further enhanced if the system reaches critical coupling. This result shows that optical mode localization-based sensing increases the sensitivity of a large cavity to the changes in refractive index, resulting in a larger shift in the amplitude of a resonant mode for a given change in refractive index, which provide a new way for ultra-sensitive fibre temperature sensing.

Funding. Engineering and Physical Sciences Research Council (EPSRC EP/V000624/1).

Acknowledgments. This work was supported by the Engineering and Physical Sciences Research Council under funding body EPSRC EP/V000624/1.

Disclosures. The authors declare no conflicts of interest

Data availability. The data that support the findings of this study are openly available at the University of Southampton ePrints research repository [26].

References

1. C. Zhao, M. H. Montaseri, G. S. Wood, S. H. Pu, A. A. Seshia, and M. Kraft, "A review on coupled mems resonators for sensing applications utilizing mode localization," Sensors Actuators A: Phys. **249**, 93–111 (2016).
2. M. Spletzer, A. Raman, H. Sumali, and J. P. Sullivan, "Highly sensitive mass detection and identification using vibration localization in coupled microcantilever arrays," Appl. Phys. Lett. **92**, 114102 (2008).
3. P. Thiruvenkatanathan, J. Yan, J. Woodhouse, and A. A. Seshia, "Enhancing parametric sensitivity in electrically coupled mems resonators," J. Microelectromechanical Syst. **18**, 1077–1086 (2009).
4. P. Thiruvenkatanathan, J. Yan, J. Woodhouse, A. Aziz, and A. Seshia, "Ultrasensitive mode-localized mass sensor with electrically tunable parametric sensitivity," Appl. Phys. Lett. **96**, 081913 (2010).
5. P. Thiruvenkatanathan, J. Woodhouse, J. Yan, and A. A. Seshia, "Limits to mode-localized sensing using micro-and nanomechanical resonator arrays," J. Appl. Phys. **109**, 104903 (2011).
6. P. Thiruvenkatanathan, J. Yan, and A. A. Seshia, "Ultrasensitive mode-localized micromechanical electrometer," in *2010 IEEE international frequency control symposium,* (IEEE, 2010), pp. 91–96.
7. P. Thiruvenkatanathan, J. Yan, and A. A. Seshia, "Common mode rejection in electrically coupled mems resonators utilizing mode localization for sensor applications," in *2009 IEEE international frequency control symposium joint with the 22nd European frequency and time forum,* (IEEE, 2009), pp. 358–363.
8. P. Thiruvenkatanathan, J. Yan, and A. A. Seshia, "Differential amplification of structural perturbations in weakly coupled mems resonators," IEEE transactions on ultrasonics, ferroelectrics, frequency control **57**, 690–697 (2010).
9. J. E. Heebner, V. Wong, A. Schweinsberg, R. W. Boyd, and D. J. Jackson, "Optical transmission characteristics of fiber ring resonators," IEEE journal quantum electronics **40**, 726–730 (2004).
10. K. Djordjev, S.-J. Choi, S.-J. Choi, and P. Dapkus, "High-q vertically coupled inp microdisk resonators," IEEE Photonics Technol. Lett. **14**, 331–333 (2002).
11. D. Rafizadeh, J. Zhang, S. Hagness, A. Taflove, K. Stair, S. Ho, and R. Tiberio, "Waveguide-coupled algaas/gaas microcavity ring and disk resonators with high finesse and 21.6-nm free spectral range," Opt. letters **22**, 1244–1246 (1997).
12. W. Bogaerts, P. De Heyn, T. Van Vaerenbergh, K. De Vos, S. Kumar Selvaraja, T. Claes, P. Dumon, P. Bienstman, D. Van Thourhout, and R. Baets, "Silicon microring resonators," Laser & Photonics Rev. **6**, 47–73 (2012).
13. H. Pi, T. Rahman, S. A. Boden, T. Ma, J. Yan, and X. Fang, "Integrated vortex beam emitter in the thz frequency range: Design and simulation," APL Photonics **5**, 076102 (2020).
14. X. Xu, H. Pi, W. Yu, and J. Yan, "On-chip optical pulse train generation through the optomechanical oscillation," Opt. Express **29**, 38781–38795 (2021).
15. H. Pi, W. Yu, J. Yan, and X. Fang, "Coherent generation of arbitrary first-order poincaré sphere beams on an si chip," Opt. Express **30**, 7342–7355 (2022).
16. P. Steglich, M. Hülsemann, B. Dietzel, and A. Mai, "Optical biosensors based on silicon-on-insulator ring resonators: A review," Molecules **24**, 519 (2019).
17. G. Liang, H. Huang, A. Mohanty, M. C. Shin, X. Ji, M. J. Carter, S. Shrestha, M. Lipson, and N. Yu, "Robust, efficient, micrometre-scale phase modulators at visible wavelengths," Nat. Photonics **15**, 908–913 (2021).
18. B. Peng, Ş. K. Özdemir, W. Chen, F. Nori, and L. Yang, "What is and what is not electromagnetically induced transparency in whispering-gallery microcavities," Nat. communications **5**, 1–9 (2014).
19. H. Pi, C. E. Campanella, D. J. Thomson, and J. Yan, "Positive and negative pull-back instabilities in mode splitting optomechanical devices," ACS Photonics **9**, 123–131 (2021).
20. F. Wang, L. Zhao, Y. Xiao, T. Li, Y. Wang, A. Soman, H. Lee, T. Kananen, X. Hu, B. P. Rand *et al.*, "Controlling microring resonator extinction ratio via metal-halide perovskite nonlinearity," Adv. Opt. Mater. **9**, 2100783 (2021).
21. J. K. Poon, J. Scheuer, S. Mookherjea, G. T. Paloczi, Y. Huang, and A. Yariv, "Matrix analysis of microring coupled-resonator optical waveguides," Opt. express **12**, 90–103 (2004).
22. T. Carmon, L. Yang, and K. J. Vahala, "Dynamical thermal behavior and thermal self-stability of microcavities," Opt. express **12**, 4742–4750 (2004).
23. H. Xu, M. Hafezi, J. Fan, J. Taylor, G. F. Strouse, and Z. Ahmed, "Ultra-sensitive chip-based photonic temperature sensor using ring resonator structures," Opt. Express **22**, 3098–3104 (2014).
24. G.-D. Kim, H.-S. Lee, C.-H. Park, S.-S. Lee, B. T. Lim, H. K. Bae, and W.-G. Lee, "Silicon photonic temperature sensor employing a ring resonator manufactured using a standard cmos process," Opt. express **18**, 22215–22221 (2010).
25. D. Presti, F. A. Videla, and G. A. Torchia, "Optical fiber ring resonator as a high-resolution spectrometer. characterization and applications with single line diode lasers," Opt. Eng. **57**, 057108–057108 (2018).
26. S. Wang, "Dataset for the paper "Optical mode localization sensing based on1 fibre-coupled ring resonators"," https://doi.org/10.5258/SOTON/D2590.